STUDY ON DISSOLUTION OF Ba-CONTAINING INOCULANT IN DUCTILE CAST IRON MELT AND NUCLEATION OF GRAPHITE

Marica Tonkovič Prijanovič
Short-cycle Higher Vocational College - Novo mesto, Novo mesto, Slovenia

Primož Mrvar and Mitja Petrič
Faculty of Natural Sciences and Engineering, Department of Materials and Metallurgy, University of Ljubljana, Ljubljana, Slovenia

Jaka Burja and Črtomir Donik
Institute of Metals and Technology, Ljubljana, Slovenia

Abstract

The production of high quality ductile cast iron requires different and complex inoculants. Besides iron and silicon, they also contain alloying elements such as zirconium, strontium, barium, calcium and rare earth metals. The addition of these elements reduces carbide solidification and increases the number of eutectic cells, which improves the quality of the cast iron produced. This study investigates the process of incipient melting of a complex barium inoculant and its effects on graphite nucleation. In the study, the sample was prepared by introducing the inoculant grain into the melt of the ductile iron. The region between the inoculant grain and the less inoculated matrix was examined metallographically using light and scanning electron microscopy. We used energy dispersion spectroscopy to determine the phases in the microstructure formed. It was found that graphite particles can already nucleate and grow in solid particles when the inoculant is still dissolving and also from the melt where the Ba and Ca concentrations are high and form $BaO \cdot CaO$ phases that serve as nuclei for graphite growth.

Keywords: *inoculant, inoculant dissolving, reaction zone, phase composition, graphite nucleation, ductile cast iron, barium inoculant*

Introduction

Various inoculants are used for the inoculation of lamellar or spheroidal cast iron. Normally, the particle size of the inoculant is smaller than 6 mm. The size of the particles used depends on how the inoculant is added to the melt. Thus, an inoculant with a larger particle size is used for inoculation in the ladle, while an inoculant with a finer particle size is added for inoculation into the melt stream on the casting line. The inoculant is added to the melt just before casting. At this molten stage, the inoculant, and the melt mix well. When the inoculant dissolves, the iron melt will then be enriched locally with Si. Since Si reduces the solubility of C, Si encourages C to come out of solution and form graphite. The addition of the inoculant has a large effect on the number of eutectic cells.[1] Alloying elements[2] and a low fading effect of the inoculant have an effect on improving the mechanical properties and machinability of the solidified casting, as the inoculant reduces the possibility of precipitation of free cementite in the casting and microporosity.[3] Therefore, these castings are more suitable for machining processes such as turning, drilling, and milling.

Development of spheroidal cast iron originates from the 1940's and the inoculation process has been the subject of research ever since. Inoculants for ductile iron are ferro-silicon-based alloys with alloying elements such as: zirconium, strontium, barium, calcium and rare earth metals.

These types of inoculants are called complex inoculants. As already mentioned, the effect of the inoculant after casting is determined by observing the cooling of the cast wedge. The tendency for chill formation does not change when complex inoculants are used, even after thirty minutes of setting.[4,5] G. Alonso and colleagues[6] studied the effect of different inoculants on the microporosity of High-Si spheroidal graphite (SG) iron. The goal of the industrial research was to assess the efficiency of eight commercial inoculants in minimizing porosity occurrence. Inoculants rich in Zr seem to produce the best results. Among these complex inoculants, commonly used in the foundry industry is also the barium-containing inoculant (FeSiBa).

It is typical of barium that it crystallizes into a body-centered cubic structure and is not soluble in iron.[7] Lux and Tannenberger[8] dealt with barium vaccines in the 1960's. They found that Ba reduces undercooling and the thickness of the chill formation in the Fe–C–Si alloy. Its effect in inoculants is seen in a more uniform distribution of graphite in the solidified cast iron.[9–11] Inoculation and the effect of inoculants on the formation of dendrites in grey cast iron has been the main preoccupation of Sun and his team of collaborators.[12] They concluded that inoculation has a great influence on the formation of finer dendrites, which play a leading role in improving the tensile strength of lamellar and spheroidal cast iron.

The effect of inoculation with commercial inoculants (Ca-FeSi, Ba, Ca-FeSi, RE-FeSi alloys) on the properties of ductile cast iron with a composition of 4.5 wt% Si was studied by Riposan and his co-workers.[13] They mainly focused on the effect of inoculants on improving the properties of nodular cast iron. It was found that a very effective inoculant is Ca, Ba-FeSi, which reduces the size of the graphite and improves its shape. Thus, the combination of barium and calcium in an inoculant (10 wt% Ba, 1 wt% Ca) makes it effective over a wider range of temperature than calcium alone and additionally,[14] the presence of barium appears to significantly reduce fading and thereby extends the holding time after inoculation.[10,15] With the addition of Ca to the melt, a part of the calcium is consumed in local deoxidation and desulfurization processes, and the rest of the calcium reacts with carbon to form calcium carbide. Due to the similarity of the lattice parameters of graphite and calcium carbide, carbide particles act as additional substrates for graphite nucleation. Similar observations were found with the use of Ba.[16] Both Ba and Ca produce more eutectic cells and lower degree of undercooling.[17,18]

Boldyreva and his co-workers[19] also analyzed barium-based inoculants. They investigated the effectiveness of inoculants with different compositions of Ba, Ca and Sr in terms of graphitization ability or a chill test. Based on their results, they assessed the quality of the different inoculants. An inoculant containing 3.3–7 wt% Ba, 2.5–4 wt% Ca and 1–2.5 wt% Al besides iron and silicon was rated best as it had the lowest chill formation layer.[19] During inoculation, Ba forms stable compounds that do not disintegrate or dissolve in the melt. The resulting compounds, which are precipitated in the form of finely dispersed particles, can form heterogeneous crystal nuclei.[4] Skaland[20] wrote about nucleation mechanisms and the heterogeneous nucleation of graphite. He put forward various theories for the nucleation of graphite, including the heterogeneous nucleation of graphite. That is, heterogeneous nucleation of graphite nuclei occurs in the Si rich regions formed in the dissolved inoculant. This reduces the solubility of the carbon and promotes the precipitation of graphite in the region where the inoculant begins to melt, precipitating tiny graphite beads. The presence of Ba has a positive effect on the precipitation graphite.

Since a lot of barium-based inoculants are used in the foundry industry, in our research we were interested in the role of Ba in the dissolution of the inoculant in spheroidal cast iron and which Ba-containing phases can act as nuclei.

Materials and Methods

To observe how the barium inoculant dissolves and the role barium plays in inoculation, we made a base cast iron in a cupola furnace. After desulfurization by CaC_2 in a desulfurization ladle and nodularization by introduction of a wire filled with FeSiMg alloy, a ductile cast iron was obtained with the composition given in Table 1. Table 1 is showing also the compositions of base alloy and desulphurized alloy. Cast iron was inoculated with a complex inoculant containing, in addition to iron, 72–77 wt% Si, 1–2 wt% Ca, 0.8–1.6 wt% Al, 2–3 wt% Ba. The particle size of the inoculant was between 2 and 6 mm.[21]

To determine the dissolution of the inoculant, a ductile cast iron melt was poured into a Quick Cup probe already filled with a tested inoculant with addition of 1.3 wt%. The grains were wrapped with a steel wire and duck tape. After

Table 1. Chemical Compositions of the Base Melt Before and After Desulphurization and After Nodularization

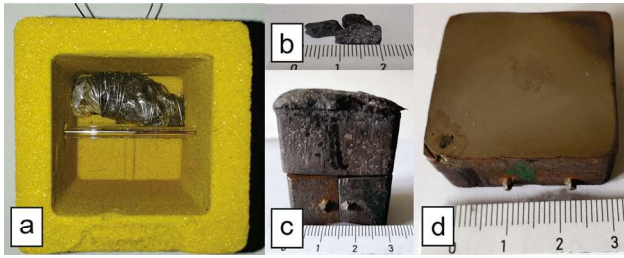| Element/wt%	C	Si	Mn	S	Cr	Mg
Before desulphurization	3.81	1.80	0.21	0.080	0.04	0.002
After desulphurization/ before nodularization	3.90	1.80	0.18	0.016	0.04	0.002
After nodularization	3.90	2.20	0.18	0.009	0.04	0.06

Figure 1. *(a) A cup for thermal analysis with an inoculant, (b) inoculant grains, (c) a casting and (d) a cross section of a sample with visible inoculant grain.*

pouring, the inoculant was placed 10 mm above the bottom on the wall of the cup. Figure 1a shows a cup prepared for thermal analysis with a barium-based inoculant attached. Figure 1b shows the 11 mm long and 6 mm wide grains of the inoculant used in the procedure. After casting the sample the specimen was cut out of the casting for metallographic observation (Figure 1c). The specimen was cut out where the inoculant was present (Figure 1d).

The microstructure was examined with the Olympus BX61 light microscope. In doing so, we analyzed the initial molten inoculant used to inoculate the ductile iron as shown in Figure 1d.

In order to view the samples under the scanning electron microscope, the metallographic samples were prepared by cross section polishing with the JEOL cross section polisher, where the surface was cut by Ar^+ ions. The prepared samples were then observed and analyzed using a field emission scanning electron microscope (FE-SEM) JEOL JSM-6500F, which was also equipped with an energy dispersion spectroscopy (EDS) detector. To determine the phases and inclusions, we performed EDS mapping and EDS line scans at 15 kV of acceleration voltage, counting time of 120 s and beam current of 5 nA. EDS and SEM analysis was also performed on the inoculant.

Results

In the study, the influence of Ba on the development of microstructure was investigated. For this purpose, the inoculant itself was analyzed under the SEM microscope. Figure 2 shows the microstructural phases of the inoculant with the corresponding chemical compositions. The eutectic is marked as spot 1. A dark phase (spot 2) is silicon. The grey phase (spot 3) is most likely $FeSi_2$. Between the grey phase and the silicon grains is a white phase (spot 5) consisting of 45.69 wt% Si, 43.74 wt% Ba, 8.84 wt% Al and 1.73 wt% Ca. The presence of the above elements is also established by an analysis marked spot 4, and this phase contains: 46.62 wt% Si, 34.73 wt% Ba, 8.8 wt% Al, 8.65 wt% Ca.

The analysis of the eutectic region (Figure 2a, spot 1) in the inoculant at higher magnifications given in Figure 2c. The eutectic consists of a white phase (spot 6) with the highest Ba content and the dark phase with the highest Ca content (spot 7). EDS analyses of both phases can be found in Figure 2d.

Figure 3 shows the non-etched microstructure in the area from the inoculant to the base microstructure with the zones of the dissolving inoculant. The inoculant, which is beginning to dissolve due to the high casting temperature (1349 °C), is visible. Between the inoculant and the cast iron there are marked passage areas—the zone where the inoculant dissolves and a reaction zone. This is where the inoculant begins to dissolve and react with the molten metal. There are various particles in these zones, which are explained below. At the boundary between the reaction zone is an accumulation of graphite in various forms, mainly irregular or exploded graphite. Further away from the reaction zone the microstructure of spheroidal cast iron is most probably less inoculated where the graphite is in the form of a nodules.

After solidification, the matrix of the ductile cast iron region contains, in addition to iron (Figure 4a), 2.40 wt% Si. The composition of the matrix gives understanding that only small amount of inoculant already dissolved in the melt which increased the Si content to the mentioned amount. If all added amount of inoculant would dissolve, the content of Si should increase for about 1 wt% in total. The graphite is in the form VI according to the standard ISO 954. Figure 4b additionally gives the cooling curve from thermal analysis from thermal center of a casting where the microstructure as presented on Figure 4a solidified.

During the investigation, we were interested in what happens to the inoculant in the dissolving and reaction zone. This was followed by SEM examination. Figure 5 shows the microstructure of the site where a fragment of the inoculant is visible. This is followed by a grey dissolving layer of the inoculant where dissolution (incipient fusion) of the inoculant and a reaction zone take place. The boundary between the dissolving inoculant and the reaction zone is marked with a black broken line.

Figure 6 shows the SEM micrograph, EDS mapping and EDS spot analyses of area A from Figure 5. The spot analysis shows the area of inoculant particles, i.e., silicon grains, $FeSi_2$ phase and eutectic, shown and discussed in Figure 2.

A phase analyzed in spot 1 (Figure 6) is enriched in Si (84.2 wt%). The other elements are Ca, Al, Ba and O where it should be mentioned that O analysis is only qualitative at EDS analysis and gives only comparative values. The analysis of spot 2 shows 46.1 wt% Fe and
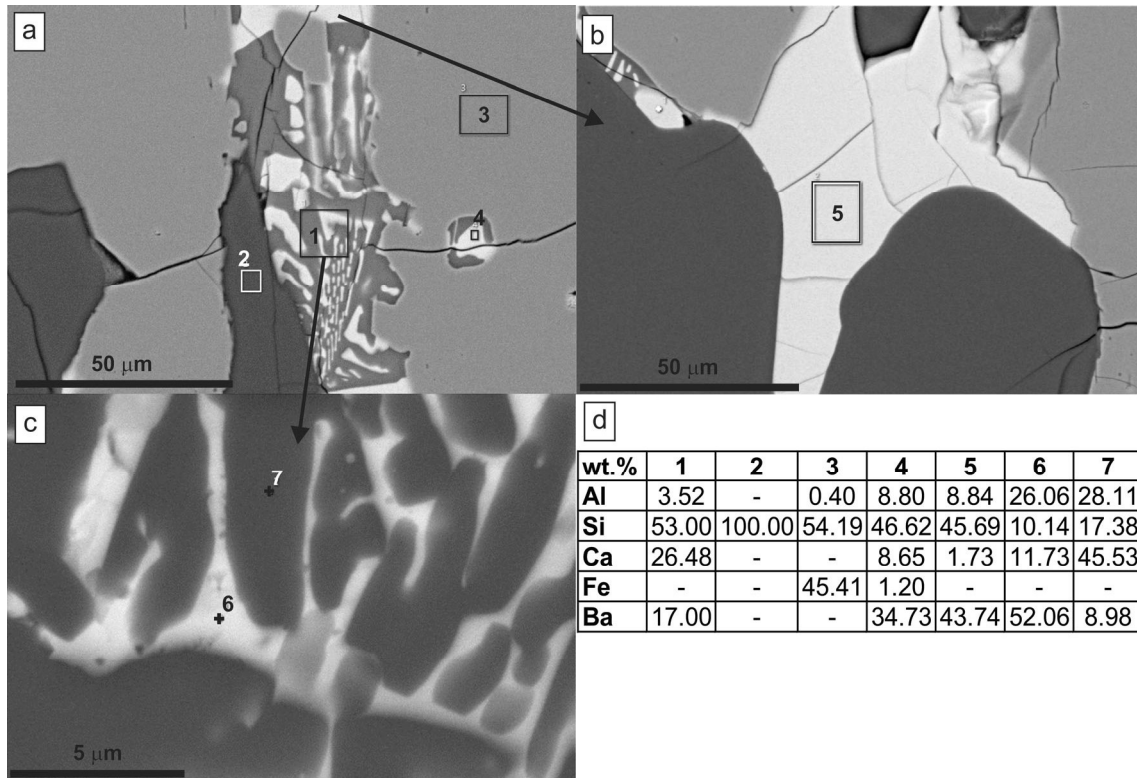
Figure 2. *(a) Microstructure of the inoculant, (b) magnified view corresponding to the marked region, (c) magnified view corresponding to marked region and (d) EDS analyses of marked spots.*
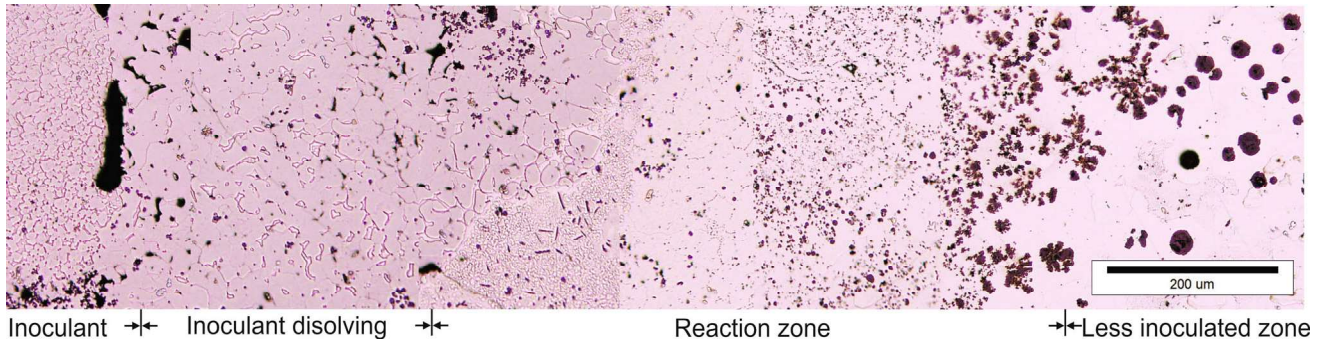
wt.%	1	2	3	4	5	6	7
Al	3.52	-	0.40	8.80	8.84	26.06	28.11
Si	53.00	100.00	54.19	46.62	45.69	10.14	17.38
Ca	26.48	-	-	8.65	1.73	11.73	45.53
Fe	-	-	45.41	1.20	-	-	-
Ba	17.00	-	-	34.73	43.74	52.06	8.98

Figure 3. *Microstructure of zones from inoculant to base nodular cast iron, not etched.*

48.9 wt% Si, i.e., a compound $FeSi_2$. Spot 3 shows the phase that is a product of a disintegrating eutectic rich in Si, Ba, Ca, Al, and O. Spot 4 is a graphite particle in contact with a phase $FeSi_2$, which is confirmed in spot 2 and the matrix (spot 5) which consists of iron (66.2 wt%) and silicon (30.9 wt%). This is interesting because the inoculant did not contain C, so it appears that C diffuses from the melt into the disintegrating inoculant particle at early stages to form graphite.

Presented in Figure 7, small particles are distributed not far from the boundary between the dissolving inoculant/

reaction zone (Figure 5, marked area B). The elemental distribution in Figure 7 shows the presence of Si phases which are in the polygonal shapes distributed independently in the matrix and are a consequence of the decomposition of the inoculant. It is evident that the temperature in this area did not reach the liquidus point of the inoculant master alloy which is between 1300 and 1325 °C.[22] Decomposition of inoculant occurs partly by dissolution and partly by disintegration, resulting in Si and Si, Fe solid intermetallic particles in the melt which had no time to dissolve into the melt. Ba-containing particles and Ca-containing particles are distributed over the surface. In the
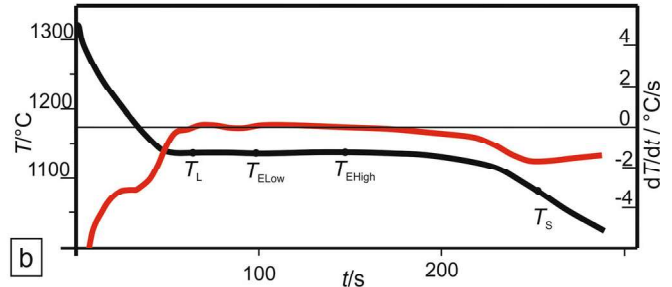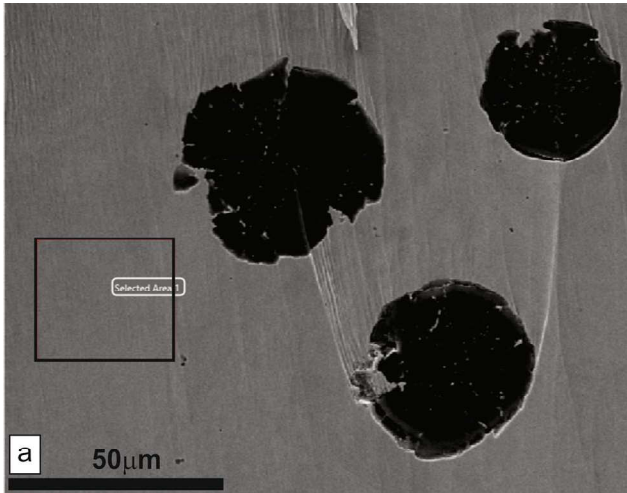
Figure 4. Shape of graphite in the less inoculated nodular cast iron with the area of EDS analysis.
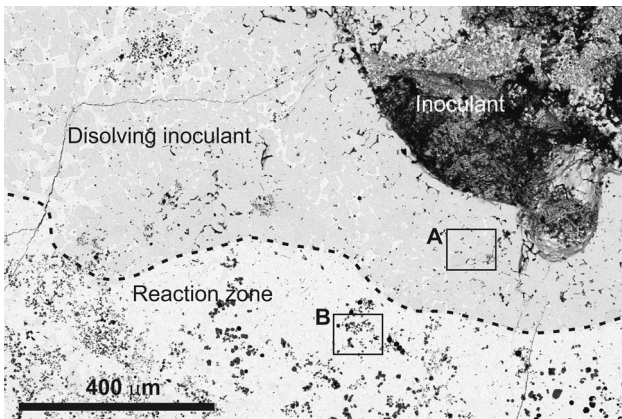

Figure 5. A micrograph of the layers of the dissolving inoculant with investigated areas.

lower right corner is FeSi$_2$, corresponding to the presence of Fe and Si. Some number of graphite particles are observed as well that appear to be nodular and placed inside Si halo. According to equilibrium Si–C phase diagram the stable SiC phase should be formed[23] and Si phase and graphite should not coexist. Similar observations were reported by the Lacaze[24] where the ternary Fe–C–Si phase diagram is presented. At Si concentrations as they are analyzed in the EDS map area from Figure 7 (17 wt% C, 19 wt% Si, Fe rest) and lower amounts of C the SiC, graphite and Fe, Si phases can exist. There is no Si phase present at such concentrations. On the other hand, Zhu et al.[25] reported about growth of Si/C microrods on a graphite substrate at temperatures of 900 °C and 1000 °C where no SiC phase is mentioned, only Si nanoparticles.

From presented results and literature the authors can refer to non-equilibrium thermodynamic conditions where solid Si is present since temperatures were estimated to reach the range of solidification of an inoculant master alloy (1200–1325 °C)[22] and Si did not dissolve. Also, the time at these temperatures was limited. It seems that C diffused

into the area from the melt and into the solid Si and formed graphite particles since temperatures were too low to form the SiC.

Figure 8 shows a more detailed image of Figure 7, a phase at the edge of the dissolving inoculant/reaction zone. A SEM micrograph shows the microstructure of the spots examined, with one particle dark grey and rich in Si (spot 2). A silicon particle contains a spherical graphite. In the vicinity of said phase there is 80.6 wt% Fe in 15.6 wt% Si. Spot 1 and Spot 3 have a similar composition, as can be seen in Figure 8b. Graphite grows within the solid silicon particles by diffusion of C atoms. The diffusion of C is estimated at around 0.95 cm^2/s, which is about 10^4 higher than in δ-Fe,[26] while the solubility is estimated at 9 × 10^{-6} mol fraction C.[27] Barium, calcium and oxygen are also frequently present and are in the form of a white phase, which is described below. Its origin is most probably from eutectics from an inoculant particle.

Figure 9 shows the distribution of elements in the reaction zone not far from the boundary of a ductile iron. Here you can see the irregularly shaped graphite in which the white phase is located, similar to Figure 8. An increased amount of Ba and Ca is present in it as well as a small amount of S. SEM micrograph with the corresponding EDS mapping of the analyzed site is shown in Figure 9a. The spot 1 of EDS analysis of the shown in Figure 9b confirms the presence of 13.3 wt% Ba and 8.7 wt% Ca and a very small amount of S which could indicate the presence of sulfide next to oxide. Spot 2 represents graphite and spot 3 represents the cast iron matrix.

The percentage of white, Ba- and Ca-containing phases increases the closer it gets to the boundary between the reaction zone and less inoculated ductile cast iron. We analyzed the precipitates from this area with a fairly large surface area. They were of different shapes, but often in the form of vermiculi. Analysis of spot 1 and 2 in Figure 10a
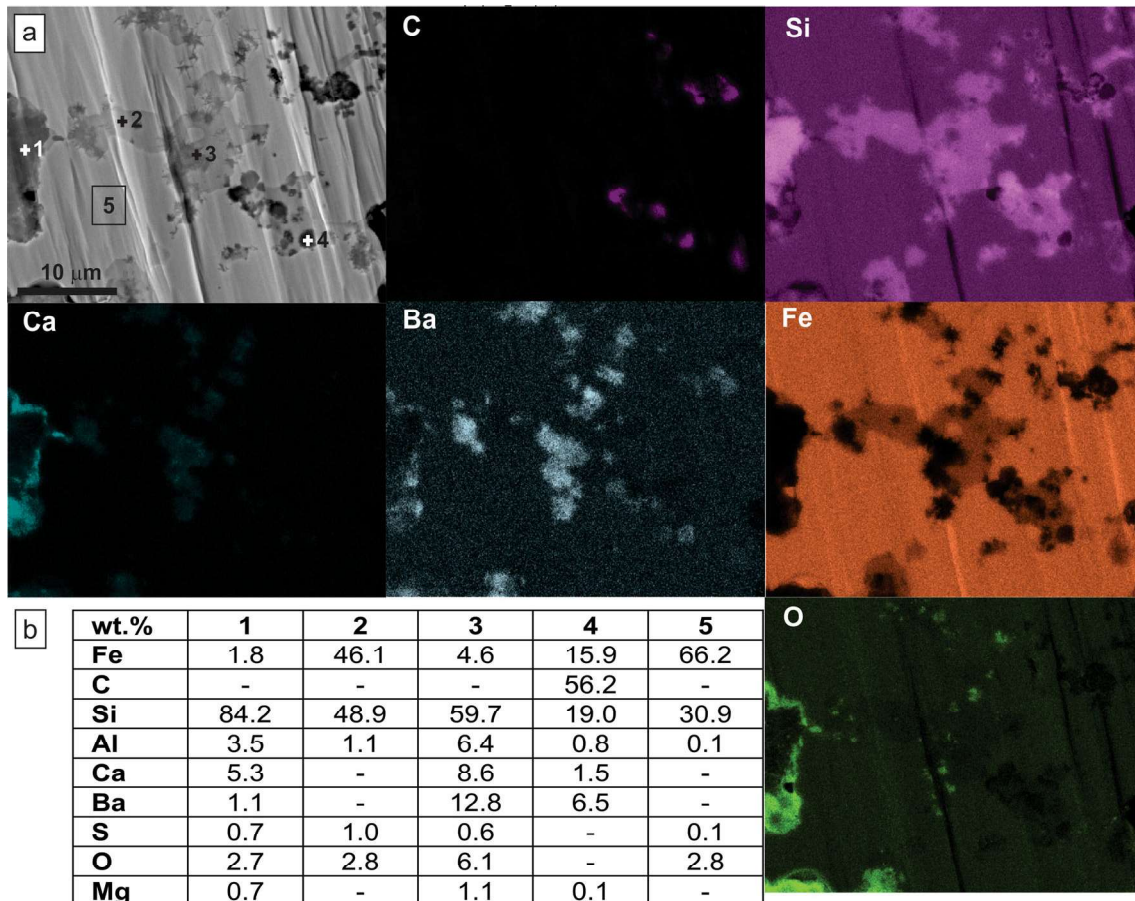
Figure 6. *EDS distribution of elements: (a) SEM micrograph EDS mapping in the area of at area A from Figure 5, (b) chemical composition of the analyzed spots in the area of incipient fusion of the inoculant.*

wt.%	1	2	3	4	5
Fe	1.8	46.1	4.6	15.9	66.2
C	-	-	-	56.2	-
Si	84.2	48.9	59.7	19.0	30.9
Al	3.5	1.1	6.4	0.8	0.1
Ca	5.3	-	8.6	1.5	-
Ba	1.1	-	12.8	6.5	-
S	0.7	1.0	0.6	-	0.1
O	2.7	2.8	6.1	-	2.8
Mg	0.7	-	1.1	0.1	-

shows that these particles consist mainly of Ba, Ca and O, no S is detected here. Considering previous studies, there is a possibility that nanoparticles could develop from $BaCaO_2$.[28] In our case, similar oxides develop as the inoculant dissolves and forms a compound BaO·CaO or $BaCaO_2$. These phases are usually located next to or inside the graphite.

Based on the results, we can confirm that the BaO·CaO phase can act as a graphite nuclei when graphite grows from the melt under the described conditions if the amounts of Ba and Ca are high enough.

Figure 10c shows the chemical composition of the different phases presented in Figure 10a, b. The particles of white color visible in the graphite and next to it are similar to the one in Figure 9. They consist of BaO·CaO (spot 1, 2, 4). Spot of analysis 3 and 8 is matrix. Spot of analysis 5 is graphite (Figure 10b). Spot 6 of analysis is most likely porosity with background analysis where Fe, Ca and Ba are also present. Spot 7 of the analysis is a bit darker than the 1, 2 and 4 and contains some Si so it may be a Ca–Ba–Si oxide.

Figure 11 shows an EDS line analysis of complex particle from Figure 10b. The analysis shows that at the transition from the cast iron matrix to the spherical graphite region, the proportion of carbon increases, while the proportion of iron decreases. In the center of the spherical graphite is a white particle. It contains Ca, Ba, O, Fe, C from which Fe and C are from the surrounding area as it is EDS analysis meaning that it must be BaO·CaO. The analyzed complex particle is also interspersed with several other smaller particles which may also have a role in graphite nucleation but the size is too low for SEM analyses.

Discussion

Based on the results presented, we have found out the sequences of graphite nucleation during inoculation with Ba-rich inoculant. The microstructure of the inoculant consists of Si and Si, Fe intermetallic phases and Ba- and Ca-rich eutectic regions. When the grain of the inoculant dissolves, it also breaks down into Si and Si, Fe intermetallic particles. The melt surrounding these particles contains C, which diffuses into area of these particles, where in many cases graphite forms on Ba- and Ca-
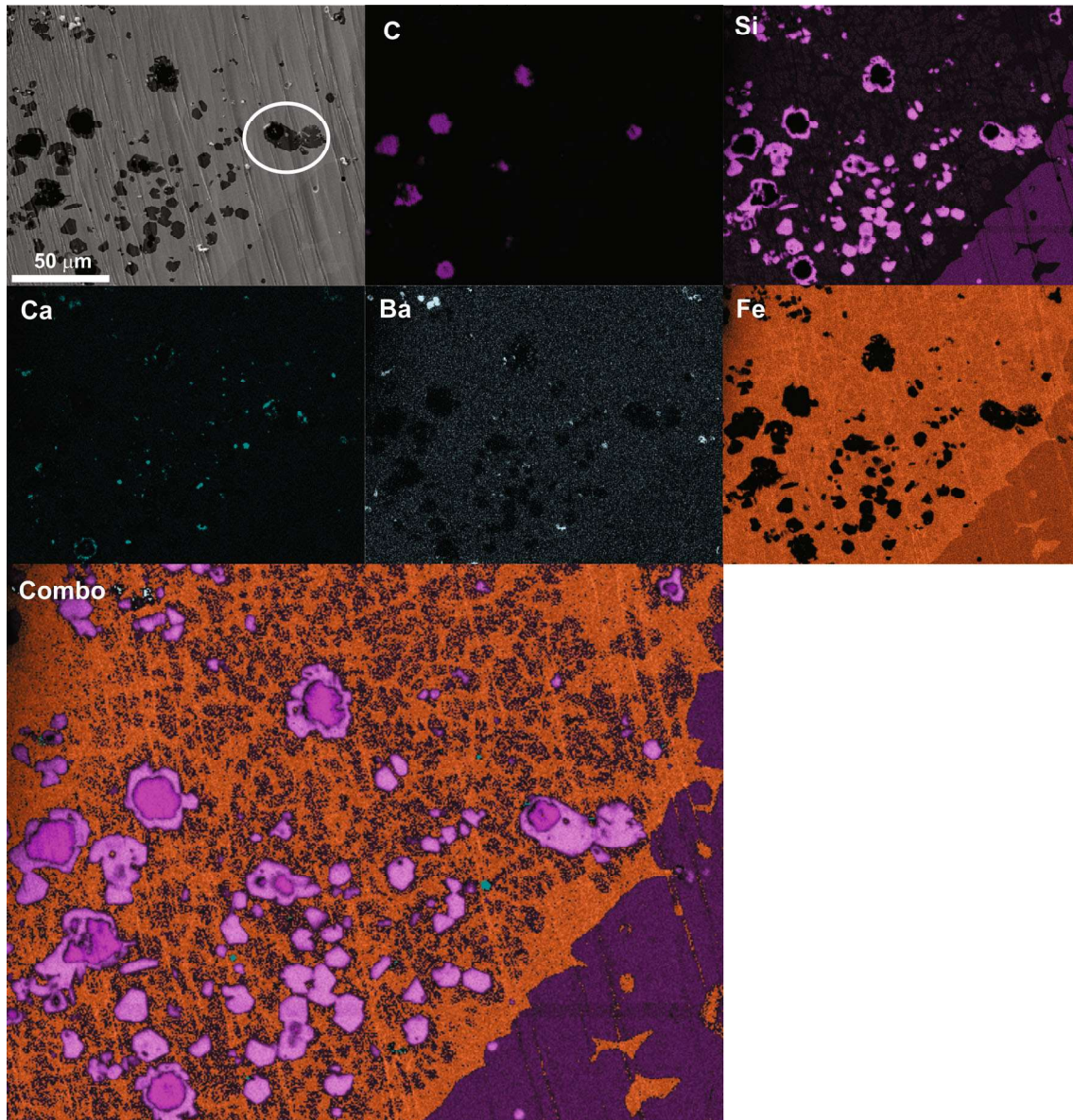
Figure 7. SEM micrograph and EDS mapping of elements at area B from Figure 5 with marked particle analyzed in Figure 8 and enlarged combo mapping.

containing particles, presumably BaO·CaO.[29–31] In our investigations, the time was limited due to the rapid cooling of the sample, so the Si phase and Si, Fe intermetallic phases did not completely dissolve. If the temperature is higher and more time is available, we assume that the Si and Si, Fe intermetallic particles would dissolve in the surrounding melt, as they are not stable in a cast iron melt. According to investigation the graphite particles also appeared with a Si halo and it is shown from the literature that diffusion of C in solid Si is plausible, but the formation of graphite is still not completely understood and further investigations are needed. Here we must consider the special circumstances under which the reactions took place between the Si rich inoculant and the C rich iron melt. The dissolution zone is therefore, the product of the reactions between the Fe–C melt (cast iron melt) and the Si rich

inoculant. The dissolution zone is enriched with Si; thus, the solubility of C in the Fe liquid is lowered. We must consider the relatively low temperatures (around 1200 °C). So, as the solubility of C is lowered, the precipitation of graphite is initiated. However, at values of more than 20 wt% Si in the melt and temperatures around 1250 °C SiC should form.[32] Furthermore, the graph on Figure 12 shows it could be possible for values of Si above 8 wt%, the values of Gibbs free energies for the formation of $C_{graphite}$ and SiC in the melt are presented. The experimental results show graphite nodules surrounded by Si (Si halo). Solid Si is not stable in the Fe based melt and should dissolve. The dissolution of solid Si particles is therefore relatively slow and any reactions that are considered between Si and C are therefore dictated by the dissolution
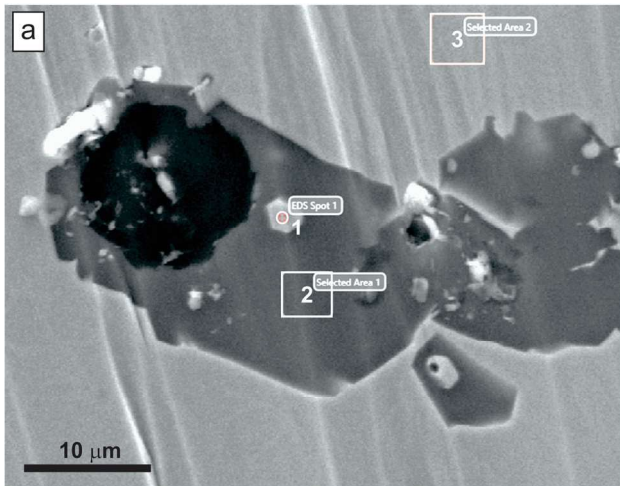
wt.%	Fe	C	Si	Al
1	80.6	-	19.0	0.4
2	1.9	-	96.6	1.5
3	80.6	3.2	15.9	0.3

Figure 8. SEM micrograph of the analyzed particle from area B of Figure 5.

of Si. So let us consider the formation SiC that can be written as:

$$[Si] + [C] = SiC$$

where [Si] and [C] are Si and C dissolved in liquid Fe at standard 1 wt%.

But the whole reaction mechanism is clearly not as simple as it seems at first glance. Silicon crystals, graphite and SiC have covalent bonds, meaning that they are strong, and are difficult to destroy. The precipitation of graphite from a C saturated Fe melt is quick, and the reaction of solid Si particles and $C_{graphite}$ would require a slow solid state reaction.[33]

We must also consider the following thermodynamic reaction for the formation of graphite:
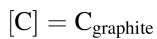
$$[C] = C_{graphite}$$

where the SiC and $C_{graphite}$ formation are therefore contending reactions.

The thermodynamic data for the reactions were taken from the literature.[34–37] The influence of the chemical composition on the activity of Si and C dissolved in liquid Fe is calculated by using first order interaction coefficients.[30,32]

$$Log fY = \sum e_Y^X \cdot (\%X), \quad Y = C, Si;$$
$$X = C, Si, Mn, S, Cr, Mg.$$

The graph for the values of Gibbs free energies for the formation graphite and SiC at 1200 °C for different Si contents are shown in Figure 12.

Furthermore when SiC is added to cast iron melt, it starts to dissolve. Experimental work has shown that the interaction layers closest to the SiC form Fe–Si phases and graphite.[38] Experiments with SiC and steel powder sintering at 1150 °C also gave similar results, producing graphite and Si rich Fe matrix.[39] Both papers mention the relatively fast dissolution of SiC, where iron diffused into the SiC and promoted SiC dissolution, with graphite formation. We must consider that the immediate Si concentration was high, but still it favored SiC disintegration into graphite and high Si iron phase.

Graphite particles present are more stable in the melt and if the temperature is low enough, they would not dissolve but if there was time to dissolve Si halo it means that these graphite particles could continue to grow into graphite during solidification.

Secondly, in the areas where the inoculant was completely dissolved, many irregularly shaped graphite particles were found next to the area that was less inoculated and, in many cases, white particles were present on or in these graphite particles. Analysis revealed that the white phases were BaO·CaO, which act as nuclei for graphite. In this area, no other phases such as other oxides, sulfides or nitrides were found in the graphite to act as nuclei as previously described.[40–42] From these results we can conclude that the BaO·CaO particles can act as nuclei for the graphite phase if the Ba and Ca concentration is high enough.

Conclusions

The present work was concerned with the study of the dissolution of Ba, Ca-containing inoculant in ductile iron and its effect on the nucleation of graphite particles. The inoculant consisted of a Si phase, a $FeSi_2$ phase and eutectic phases rich in Si, Ba, Ca and Al. The reaction zone of the dissolving inoculant particle was about 1.5 mm thick. From this distance, the structure was no longer inoculated or it was under inoculated.

In between was the dissolution zone, where the dissolving inoculant particle produced phases like those of the inoculant itself. In this layer, dissolution and the breakdown of inoculant particle took place, resulting in Si phase and Si, Fe intermetallic phases in the microstructure. Graphite grew on interfaces of Si, Fe intermetallic phases. In Si particles, the graphite grew inside the solid Si by diffusion processes. This phenomenon needs further investigations for better understanding how graphite can grow inside the solid Si. In the areas further away from inoculant particles the graphite has an irregular shape that grows from the melt and contains BaO·CaO particles that serve as nuclei for graphite.
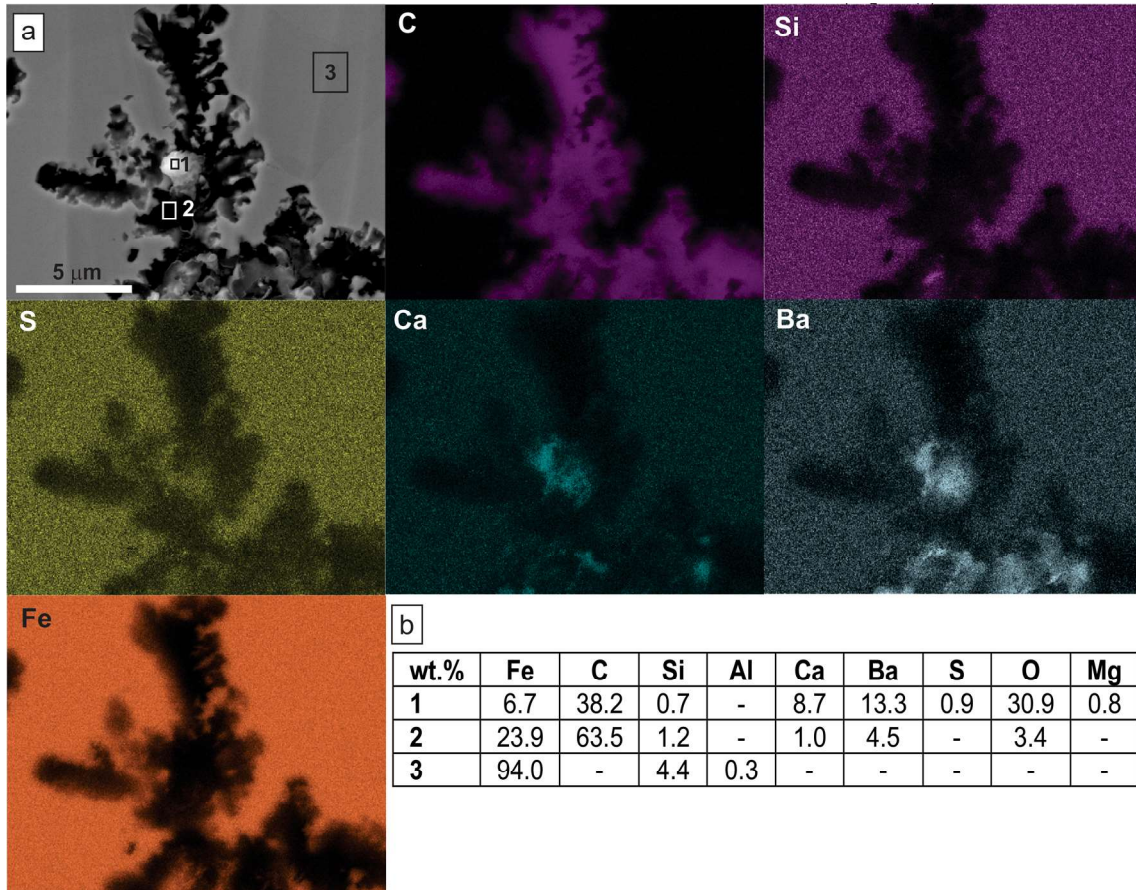
Figure 9. *(a) SEM micrograph with EDS mapping of elements in the reaction zone, (b) chemical analysis of marked particles.*
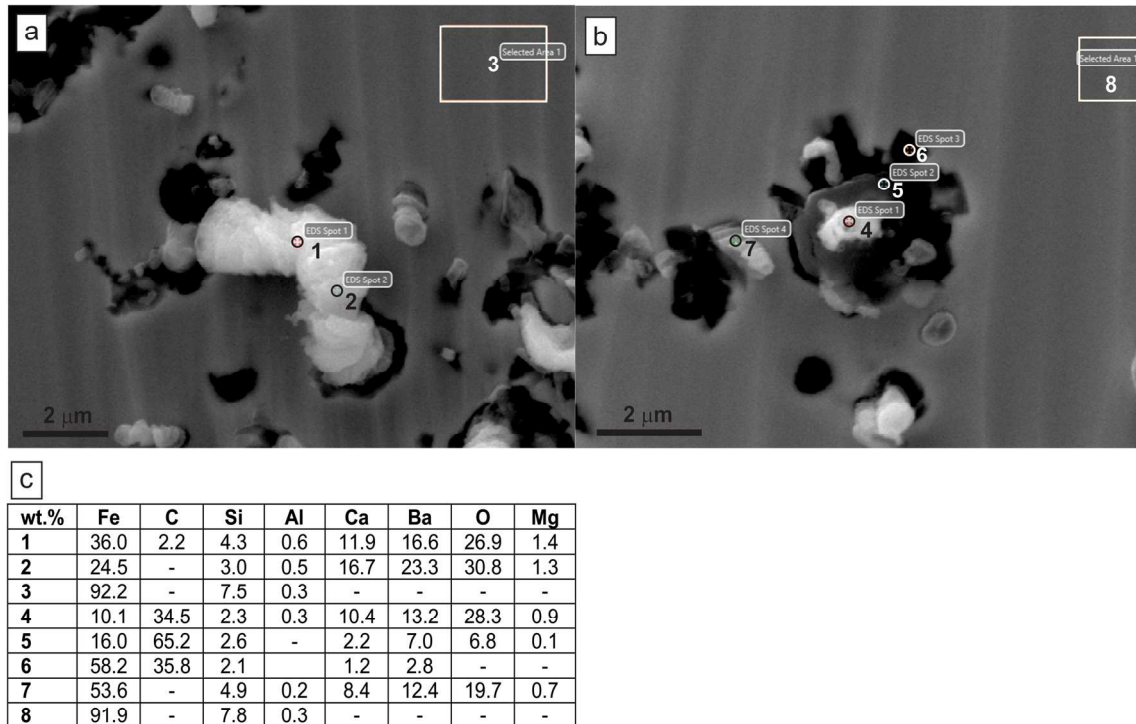
wt.%	Fe	C	Si	Al	Ca	Ba	S	O	Mg
1	6.7	38.2	0.7	-	8.7	13.3	0.9	30.9	0.8
2	23.9	63.5	1.2	-	1.0	4.5	-	3.4	-
3	94.0	-	4.4	0.3	-	-	-	-	-

wt.%	Fe	C	Si	Al	Ca	Ba	O	Mg
1	36.0	2.2	4.3	0.6	11.9	16.6	26.9	1.4
2	24.5	-	3.0	0.5	16.7	23.3	30.8	1.3
3	92.2	-	7.5	0.3	-	-	-	-
4	10.1	34.5	2.3	0.3	10.4	13.2	28.3	0.9
5	16.0	65.2	2.6	-	2.2	7.0	6.8	0.1
6	58.2	35.8	2.1		1.2	2.8	-	-
7	53.6	-	4.9	0.2	8.4	12.4	19.7	0.7
8	91.9	-	7.8	0.3	-	-	-	-

Figure 10. *(a, b) SEM micrographs of BaO·CaO particles in graphite, (c) EDS analyses of analyzed spots.*
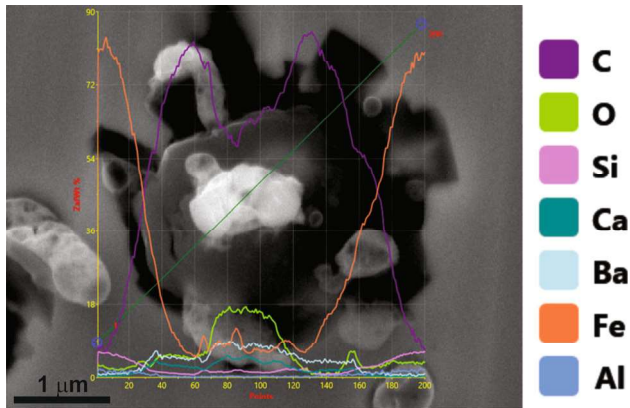
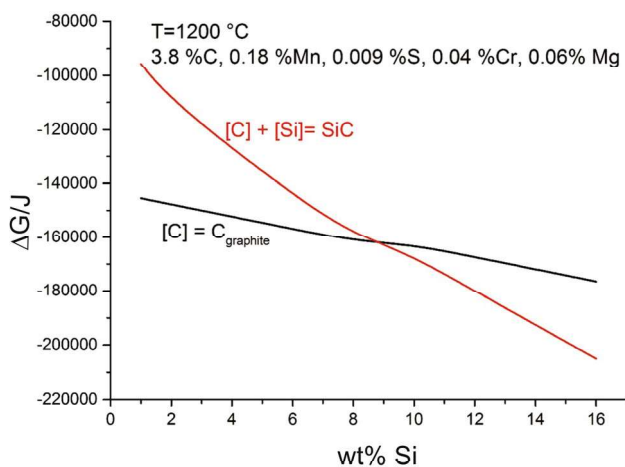**Figure 11. Line EDS analysis of graphite.**

Figure 12. Gibbs free energies for the formation of $C_{graphite}$ and SiC in Fe melt (with the final composition given in Table 1) at 1200 °C.

The most important result of the presented research is that BaO·CaO particles can act as graphite nuclei if the concentration of Ba and Ca is high enough in example at conditions next to inoculant dissolution. Apart from other research reporting on different phases acting as nuclei, we have found nothing like this since the normal inoculation conditions give much lower concentrations of Ba and Ca.

Funding

Conflict of interest The authors have no competing interests to declare that are relevant to the content of this article.

Open Access

REFERENCES

1. R.A. Harding, J. Campbell, N.J. Saunders, in *An Assessment of Our Current Understanding of the Inoculation of Cast Iron* (AFS Congress, 1998)
2. B. Bauer, P.I. Mihalic, M. Petrič et al., Effect of Si and Ni addition on graphite morphology in heavy section spheroidal graphite iron parts. Mater. Sci. Forum **925**, 70–77 (2018). https://doi.org/10.4028/www.scientific.net/MSF.925.70
3. S.N. Lekakh, Effect of nonmetallic inclusions on solidification of inoculated spheroidal graphite iron. Int. Metalcast. **13**, 47–57 (2019). https://doi.org/10.1007/s40962-018-0243-2
4. C. Pelhan, Reakcije pri cepljenju s kompleksnim modifikatorjem FeSiBa. Livarski vestnik **2**, 34 (1985)
5. S.O. Olsen, T. Skaland, Inoculation of grey and ductile iron. (Elkem, Norway, 2022), https://akademi.tudoksad.org.tr/site/file?u=20181210104117_congress_file_262.pdf&t=INOCULATION+OF+GREY+AND+DUCTILE+IRON. Accessed 1 Oct 2022
6. G. Alonso, D.M. Stefanescu, J. Sanchez et al., Effect of the type of inoculant on the shrinkage porosity of high-silicon SG iron. Int. Metalcast. **16**, 106–118 (2022). https://doi.org/10.1007/s40962-021-00605-8
7. Ba-Fe, https://www.crct.polymtl.ca/fact/phase_diagram.php?file=Ba-Fe.jpg&dir=FTlite. Accessed 5 Oct 2022
8. B. Lux, H. Tannenberger, Inoculation effect on graphite formation in pure Fe–C–Si. Mod. Cast. **3**, 57–59 (1962)
9. D. Patel, P.K. Nanavati, C.M. Chug, in *National Conference on Emerging trends in Engineering Technology and Management*", Effect of Ca and Ba Containing Ferrosilicon Inoculants on Microstructure and Tensile Properties of IS-210, and IS-1862 Cast Irons (Ahmedabad, 2013), pp. 1–8, https://www.researchgate.net/publication/289175505. Accessed 10 Oct 2022
10. D.M. Stefanescu, Inoculation of ductile iron with Barium and Cerium alloys. AFS Cast Met. Res. J. **9**, 8–13 (1973)

11. D.M. Stefanescu, Vergleich zwischen der Impfwirkung von Natrium und Barium. Giesserei-Praxis **24**, 429–433 (1972)

12. G.X. Sun, X.M. Zhu, Z.D. Lu et al., The effect of inoculant on the structure and properties of gray iron. Int. J. Cast Met. Res. **11**(5), 363–367 (2016). https://doi.org/10.1080/13640461.1999.11819300

13. I. Riposan, E. Stefan, S. Stan et al., Effects of inoculation on structure characteristics of high silicon ductile cast irons in thin wall castings. Metals **10**(8), 1091 (2020). https://doi.org/10.3390/met10081091

14. L. Michels, A.J.F. Pires, C.A.S. Ribeiro, B. Kroka, E.G. Hoel, E. Ott, C. Hartung, Effect of holding time on populations of microparticles in spheroidal graphite irons. Metall. Mater. Trans. B **53**, 836–847 (2022). https://doi.org/10.1007/s11663-021-02418-w

15. A. Fay, P. Pinel, Inoculation solutions against metallurgical problems. Int. Metalcast. **14**, 1123–1135 (2020). https://doi.org/10.1007/s40962-020-00431-4

16. E. Fraś, M. Górny, Inoculation effects of cast iron. Arch. Foundry Eng. **4**, 39–46 (2012). https://doi.org/10.2478/v10266-012-0104-z

17. S. Lekakh, C.R. Loper, Improving inoculation of ductile iron. AFS Trans. **111**(05), 885–894 (2003)

18. D.M. Stefanescu, G. Alonso, R. Suarez, Recent developments in understanding nucleation and crystallization of spheroidal graphite in iron-carbon-silicon alloys. Metals **10**(2), 221 (2020). https://doi.org/10.3390/met10020221

19. D. Boldyreva, R. Dema, O. Kalugina, Research of phase composition of graphitizing ferro silicon barium inoculants. Mater. Today Proc. **11**(1), 510–515 (2019). https://doi.org/10.1016/j.matpr.2019.01.022

20. T. Skaland, in *Proceedings of the AFS Cast Iron Inoculation Conference*. Nucleation Mechanisms in Ductile Iron (2005), pp. 12–21

21. Nodularisers, Elkem, https://www.elkem.com/silicon-products/iron-foundries/nodularisers/. Accessed 1 Sept 2022

22. Barinoc-Inoculant, Elkem, https://www.yumpu.com/en/document/read/50311853/barinocr-inoculant-elkem. Accessed Oct 2023

23. V. Haase et al., The Si–C phase diagram, in *Si Silicon. Gmelin Handbook of Inorganic Chemistry/Gmelin Handbuch der Anorganischen Chemie*, vol. S-i/B/1-5/3, ed. by H. Katscher, R. Sangster, F. Schröder (Springer, Berlin, 1985). https://doi.org/10.1007/978-3-662-06994-3_1

24. J. Lacaze, B. Sundman, An assessment of the Fe–C–Si system. Metall. Trans. A **22a**, 2211–2223 (1991)

25. X. Zhu, Y. Wang, H. Chen, Q. Tan et al., Growth of silicon/carbon microrods on graphite microspheres as improved anodes for lithium-ion batteries. J. Mater. Chem. A **1**, 4483–4489 (2013)

26. P. Werner, U. Gösele, H.J. Gossmann, D.C. Jacobson, Appl. Phys. Lett. **73**, 17 (1998). https://doi.org/10.1063/1.122483

27. F. Durand, J.C. Duby, J. Phase Equilib. **20**, 1 (1999). https://doi.org/10.1361/105497199770335956

28. K. NagendraNaik, K. Yogendra, K.M. Mahadevan, Solution combustion synthesis of $BaCaO_2$ nanoscale metal oxide and photocatalysisof methyl violet 10b dye. J. Crit. Rew. **4**(7), 2259–2265 (2020)

29. MME 3514 Materials thermodynamics, Chemical Reaction Equilibria Continued, https://bap.mu.edu.tr/icerik/metalurji.mu.edu.tr/Sayfa/MME%203514%20-%20Course10.pdf. Accessed March 2023

30. M.D. Johnston, L.T. Khajavi, M. Li et al., High-temperature refining of metallurgical-grade silicon: a review. JOM **64**, 935–945 (2012). https://doi.org/10.1007/s11837-012-0384-3

31. R. Zhang, P. Taskinen, A thermodynamic assessment of the BaO–MgO, BaO–CaO, BaO–Al_2O_3 and BaO–SiO_2 systems (Aalto University publication series, SCIENCE + TECHNOLOGY4/2014, Helsinki, 2014), p 24

32. D.M. Stefanescu, *ASM Metals Handbook, Volume 15 - Casting*, 9th edn. (ASM International, Metals Park, 1998)

33. T. Nakamura, K. Shimizu, J. Osugi, Rev. Phys. Chem. Jpn. **39**, 2 (1969)

34. G.K. Sigworth, J.F. Elliott, Met. Sci. **8**, 298–310 (1974). https://doi.org/10.1179/msc.1974.8.1.298

35. J.B. McBride, G. Sanford, M.A. Reno, NASA Technical Memorandum 4513 (1993)

36. G.V. Belov, V.S. Iorish, V.S. Yungman, Calphad **23**, 2 (1999). https://doi.org/10.1016/S0364-5916(99)00023-1

37. L.V. Gurvich, I.V. Veyts, C.B. Alcock, *Thermodynamic properties of individual substances*, 4th edn. (Hemisphere, New York, 1990)

38. T. Semleit, I. Adhiwiguna, J. Wijaya, Giesserei, 1 (2021)

39. N. Araya, G.O. Neves, A.I. Ramos Filho, C. Aguilar, J.D. Biasoli de Mello, C. Binder, A.N. Klein, G. Hammes, Mater. Chem. Phys. (2020). https://doi.org/10.1016/j.matchemphys.2020.123442

40. M.P. Tonkovič, P. Mrvar, M. Vončina et al., Analysis and thermodynamic stability of nuclei in spheroidal graphite in Fe–C–Si alloys. Mater. Technol. **4**, 533–539 (2021). https://doi.org/10.17222/mit.2021.063

41. Y. Igarashi, S. Okada, Observation and analysis of the nucleus of spheroidal graphite in magnesium-treated ductile iron. Int. J. Cast Met. Res. **2**, 83–88 (1998). https://doi.org/10.1080/13640461.1998.11819261

42. G. Alonso, P. Larranñaga, E. de la Fuente et al., Kinetics of nucleation and growth of graphite at different stages of solidification for spheroidal graphite iron. Int. Metalcast. **11**, 14–26 (2017). https://doi.org/10.1007/s40962-016-0094-7